

DeepScaffold: a comprehensive tool for scaffold-based de novo drug discovery using deep learning

Yibo Li,^{†,‡,¶} Jianxing Hu,^{†,¶} Yanxing Wang,[†] Jielong Zhou,^{*,‡} Liangren Zhang,^{*,†}
and Zhenming Liu^{*,†}

[†] *State Key Laboratory of Natural and Biomimetic Drugs, School of Pharmaceutical Sciences, Peking University, Xueyuan Road 38, Haidian District, 100191, Beijing, China*

[‡]*Stonewise, Beijing, China*

[¶]*Contributed equally to this work*

E-mail: zhoujielong@stonewise.cn; liangren@bjmu.edu.cn; zmliu@bjmu.edu.cn

Abstract

The ultimate goal of drug design is to find novel compounds with desirable pharmacological properties. Designing molecules retaining particular scaffolds as the core structures of the molecules is one of the efficient ways to obtain potential drug candidates with desirable properties. We proposed a scaffold-based molecular generative model for scaffold-based drug discovery, which performs molecule generation based on a wide spectrum of scaffold definitions, including BM-scaffolds, cyclic skeletons, as well as scaffolds with specifications on side-chain properties. The model can generalize the learned chemical rules of adding atoms and bonds to a given scaffold. Furthermore, the generated compounds were evaluated by molecular docking in DRD2 targets and the results demonstrated that this approach can be effectively applied to solve several drug

design problems, including the generation of compounds containing a given scaffold and de novo drug design of potential drug candidates with specific docking scores. Finally, a command line interface is created.

Introduction

"Molecular scaffold" is one of the most important and widely used concept in medicinal chemistry. Given a chemical compound, its "scaffold" generally represents the core structures of the molecular framework.¹ Although various definition of molecular scaffold are available, the most widely adopted version is given by Bemis and Murcko,² who obtain the scaffold by removing all side chains (or R-groups). Among all scaffolds, those with preferable bioactivity properties (which are referred to as "privileged scaffolds"³ or "bioactive scaffolds"^{4,5}) are of particular interest to drug discovery. Privileged scaffolds are often used as a starting point for compound synthesis or diversification. Previous researches have developed various types of tools to extract and utilize information from scaffolds, including tools for the discovery of privileged scaffolds (such as CSE⁶ and⁵), tools for organizing scaffolds (such as HierS,⁷ SCONP,⁸ ST⁹ and SN⁴), as well as tools for visualization (such as Scaffold Hunter¹⁰).

Recently, deep learning¹¹ have revealed itself as a new and promising tool for many drug-design-related problems. In particular, there is a growing interest in using deep generative models¹² for *de novo* molecule design.¹³ Early works in this area¹⁴⁻¹⁶ mainly utilizes RNN based architectures (such as GRU¹⁶ or LSTM¹⁴) to generate SMILES strings,¹⁷ which is a serialized representation of molecules graph. Those methods have proven to be very effective for *de novo* molecule design, but still faces certain issues, such as the need to learn SMILES grammar. Recent works¹⁸⁻²² have improved upon this approach by using graph based representation of molecules. Also, other types of generative architecture have also been explored, such as GAN.²³ Those models have been successfully applied to various drug design problems, such as property-based design of virtual libraries,^{16,18} ligand^{14,16,18} and structural²⁴ based drug design, as well as local optimization of molecular structures.^{16,22}

With the promising performance, it is natural to apply deep generative models to scaffold directed drug design. Early works have used conditional generative model,¹⁸ reinforcement learning¹⁸ or transfer learning²⁵ to achieve molecule generation based on scaffold queries. However, those methods do not guarantee that the outputs molecule will match the input query, and are difficult to be extended to new scaffolds. A recent publication by Lim et. al.²⁶ solved the problems above using a model that directly grow molecules on the given scaffold. However, the model is restricted only to BM-scaffolds, which does not necessarily fit well with all tasks in medicinal chemistry.

In this work, we introduce DeepScaffold, a novel and comprehensive solution for scaffold-based drug discovery. Different from previous methods, DeepScaffold can perform molecule generation based on a wide spectrum of scaffold definitions, including BM-scaffolds, cyclic skeletons, as well as scaffolds with specifications on side-chain properties. Our proposed method can guarantee that the output molecule would match the scaffold query, and can be easily extended to new scaffolds outside the training set. A broad set of evaluation is carried out to assess the performance of DeepScaffold. We also discuss several challenges faced when evaluation such scaffold-based generative models. Finally, a command line interface is created for DeepScaffold, as well as a docker image to facilitate deployment and scaling. The source code for this project is available at [repo]

Methods

An overview of DeepScaffold

Before diving into the implementation details, we first take a look of the overall architecture of DeepScaffold. As mentioned earlier, DeepScaffold is capable of performing de novo drug design based on the following scaffold definitions (Figure1):

- Cyclic skeletons

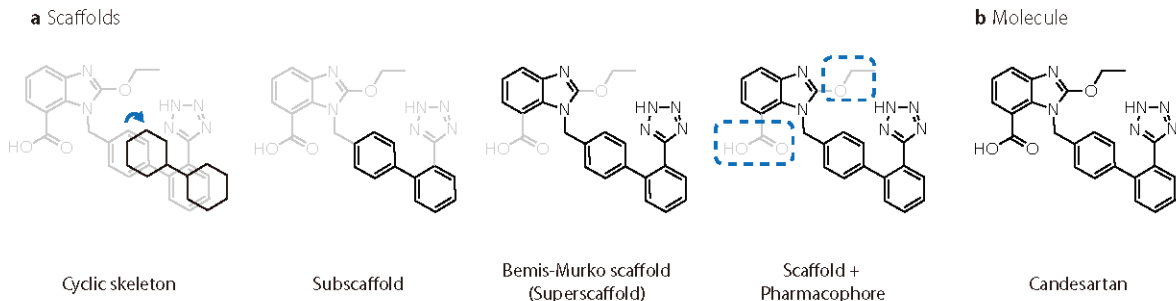


Figure 1: An overview of DeepScaffold. DeepScaffold is a comprehensive tool for scaffold-directed drug discovery, capable of performing molecule generation based on **a.** cyclic skeletons (CSKs), **b.** classical molecular scaffolds, such as Bemis-Murko scaffolds, as well as **c.** scaffolds with additional pharmacophore-based queries for side chains.

- Scaffolds with atom and bond type information, such as Bemis-Murko scaffold
- Scaffolds with additional specification on side-chain properties

For convenience, we refer to the first type of structures as the “skeletons”, and the second type of structure as the “classical scaffolds”. To achieve those functionalities, DeepScaffold is composed of the following three components:

- A neural network for completing atom and bond type for cyclic skeletons (Figure 2a)
- A scaffold-based molecule generator (Figure 2b)
- A filter based on side-chain properties (Figure 2c)

The three components are discussed in detail in the rest part of this section. We first discuss the dataset and data processing workflow in . The transformer from skeletons to scaffolds is discussed in , and the scaffold-based generator is discussed in . Finally, the evaluation methods are discussed in .

Dataset

For model training, we use molecules from ChEMBL,²⁷ which is a widely used database containing both structural and bioactivity information for molecules. The data processing

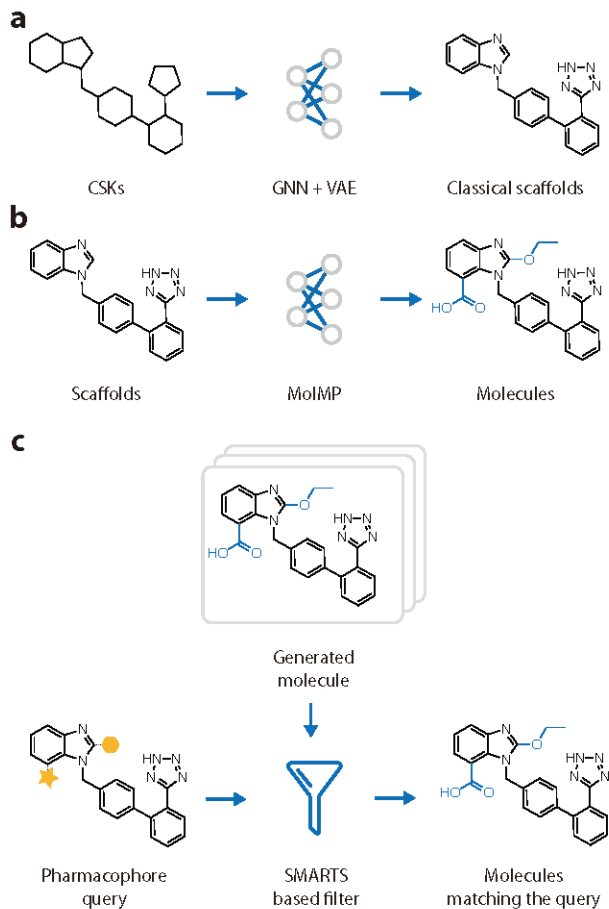


Figure 2: The basic components for DeepScaffold. As shown in the figure, DeepScaffold is composed of the following three models: **a**. A neural network for completing atom and bond type for cyclic skeletons; **b**. A scaffold-based molecule generative model; **c**. A filter based on side-chain properties

workflow largely follows that used in our previous study.¹⁸ First of all, the structural information of molecules represented as canonical SMILES are first extracted from ChEMBL dataset. The molecules are then standardized using RDKit, which involves the removal of salt and isotopes, as well as charge neutralization. Molecules containing elements outside the set {H, C, N, O, F, P, S, Cl, Br, I} are filtered from the dataset. In addition, to make the dataset more suitable for drug design purposes, we only keep molecules with QED²⁸ larger than 0.5. The final dataset (denoted as $\mathcal{M} = \{m_i\}_{i=1}^{N_m}$) contains $N_m = 914464$ molecules. The distribution of several important molecular properties (including MW, LogP, QED and SAScore²⁹) are visualized in Figure 3.

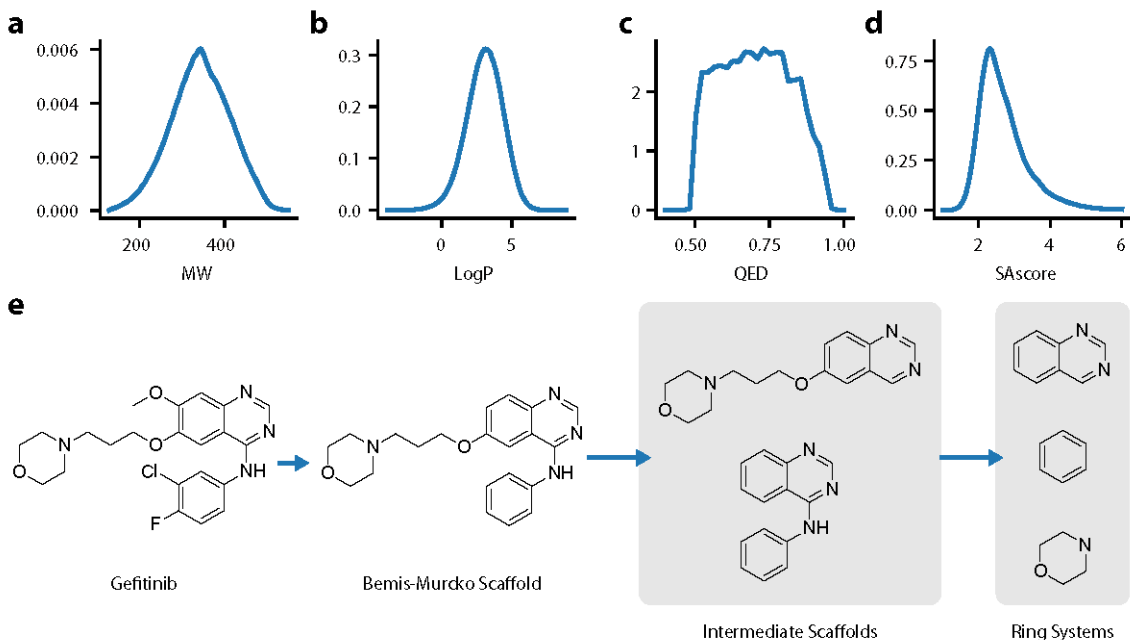


Figure 3: a-d. The distribution of several important molecular properties (a for MW, b for LogP, c for QED, d for SAScore) of the extracted molecules. e. Workflow for scaffold extraction. Given the input molecule, the Bemis-Murcko scaffold is first extracted by removing all side chains. Other scaffolds are then obtained by recursively removing ring systems.

After the dataset is obtained, we need to extract scaffolds from each molecule. Previous researchers have developed many different ways to extract and organize scaffolds from structural data. Examples include HierS,⁷ SCONP,⁸ scaffold tree (ST)⁹ and scaffold network (SN).⁴ Here, we adopt the same scaffold extraction method as HierS. Compared with ST and SN, which are more widely adopted, HierS results in a fewer amount scaffolds, but is much easier to implement.

Molecules are composed of three components: ring systems (ring), side-chain bonds and atoms (chain), and linking bonds and atoms (linker). Atoms that are external to a ring but are bonded to a ring atom with a bond order greater than 1 are to be part of the ring system because they modify the nature of the ring. Atoms that are double-bonded to linker atoms are also considered to be part of the linker because they can modify the nature of the linker. The basis scaffolds for a molecule are the set of all unique ring systems in the molecule, where a ring system is defined as one or more rings that share an internal bond.

A recursive algorithm is used to elucidate all candidate scaffold structures including those derived from exhaustive combinations of the basis scaffolds. It recursively removes each ring system from the scaffolds of each level to generate fragments that contain all possible ring system combinations. Finally, the process is completed by adding the Bemis-Murko scaffold of the compound to the list of scaffold structures.

After all the distinct basis and multi-ring system scaffolds for each molecule have been identified and added to the scaffold list, hierarchical structural relationships between the scaffolds ($s \in \mathcal{S}$) and original compound ($m \in \mathcal{M}$) structures are established. Once all scaffolds are identified and their hierarchical relationships are established, the process can rapidly traverse the network of structural connections to determine relationships between indices of scaffolds and its original compounds.

In addition, to facilitate the sampling of training data during model optimization, we created indexes between skeletons ($c \in \mathcal{C}$), scaffolds ($s \in \mathcal{S}$) and molecules ($m \in \mathcal{M}$). Specifically, indexes are created:

- From a given scaffold s to its corresponding skeleton $c(s)$.
- From a given scaffold s to the set of all molecules containing that scaffold $\mathcal{M}(s)$
- From a given molecule m to the set of its sub-scaffolds $\mathcal{S}(m)$

Generating scaffolds from cyclic skeletons

As discussed in , in order to generate molecules from a given cyclic skeleton (CSK), we need to first generate a scaffold with atom types and bond types. In order to achieve this goal, we need to model a conditional distribution $p_{\theta}(G_s|G_c)$, where G_c is the molecular graph of CSK c , and G_s is the graph of the classical scaffold s . We construct the process as follows (see Figure 4):

- We first attach to each atom v and bond e in c a latent variable sampled from a prior

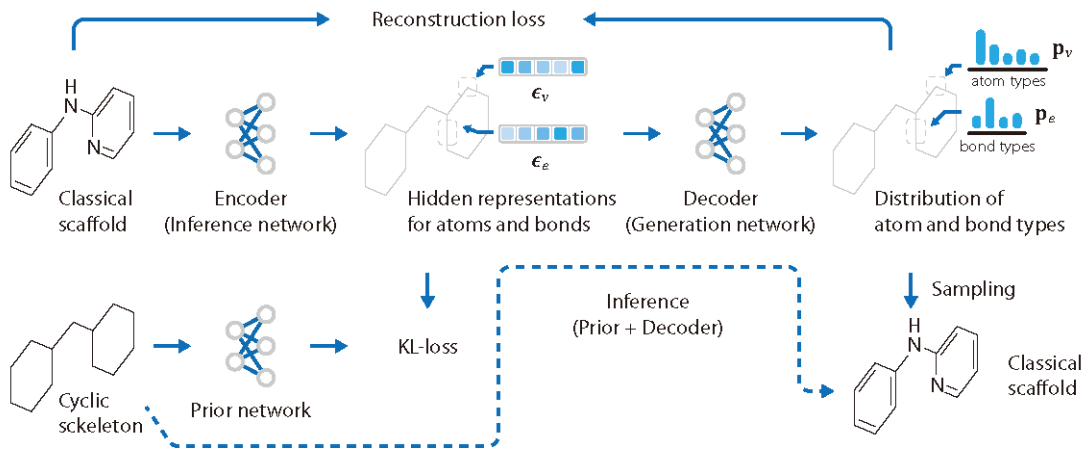


Figure 4: The architecture of the model to transform CSKs to classical scaffolds. Under the context of autoencoder, the entire model contains three components: the encoder, the decoder, and the prior network. During training, the reconstruction loss $\mathcal{L}_{\text{recon}}$ and the KL loss \mathcal{L}_{KL} are calculated using the encoder, decoder and prior for model optimization. During inference, the latent variable is first sampled from the prior network, and then fed into the decoder (or the generator network) to produce the classical scaffold.

distribution $\epsilon_v, \epsilon_e \sim p_{\theta}(\epsilon|G_c)$. Here, we use a gaussian distribution with diagonal covariance structure to parameterize the prior: $p_{\theta}(\epsilon|G_c) = \mathcal{N}(\epsilon; \mu_{\theta}^{\text{prior}}(G_c), \sigma_{\theta}^{\text{prior}}(G_c)^2 \mathbf{I})$

- The latent variables ϵ_v, ϵ_e , together with the topological structure of the CSK, is feed into a graph convolutional neural network to generate a probability distribution of atom types for each node \mathbf{p}_v and bond types for each edge \mathbf{p}_e .
- The types of each atom and bond in the output scaffold s are then sampled from the distributions \mathbf{p}_v and \mathbf{p}_e .

The latent variables are necessary to capture the probabilistic dependencies between different atoms and bonds. For convenience, we let $\epsilon_V = [\epsilon_v]_{v \in V}$, $\epsilon_E = [\epsilon_e]_{e \in E}$, and $\epsilon = [\epsilon_V, \epsilon_E]$. Under the construction above, we can write the conditional distribution $p_{\theta}(G_s|G_c)$ as:

$$p_{\theta}(G_s|G_c) = \int_{\epsilon} p_{\theta}(G_s|G_c, \epsilon) p_{\theta}(\epsilon|G_c) \quad (1)$$

A straight forward way of training such model is to maximize its likelihood value. However, as the model contains latent variables, calculating its likelihood value is not directly

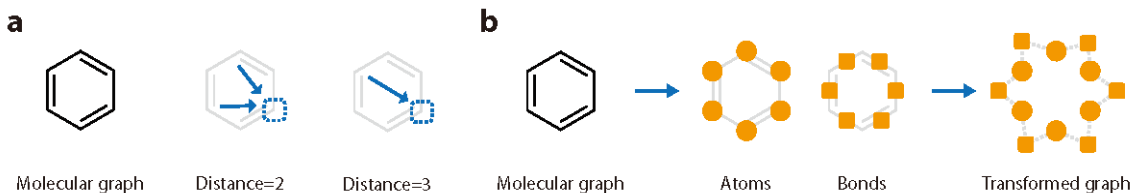


Figure 5: The architecture of the graph convolutional neural network (GNN). Before feeding into the GNN, two transformations are performed on the original molecular graph G : **a.** Virtual bonds are added to capture remote connectivity relationship. **b.** The atoms and bonds are treated equally as "nodes" in the new graph.

feasible. Therefore, we use variational inference to obtain a lower-bound of the likelihood. Specifically, we reformulate the model as a variational autoencoder³⁰ by adding an auxiliary inference network $q_{\theta}(\epsilon|G_s, G_c)$ to the model. Since G_s already contains the full information of G_c , we shall write the inference network as $q_{\theta}(\epsilon|G_s)$. Similar to the prior, we use a diagonal Gaussian distribution for q_{θ} : $q_{\theta}(\epsilon|G_s) = \mathcal{N}(\epsilon; \mu_{\theta}^{\text{post}}(G_s), \sigma_{\theta}^{\text{post}}(G_s)^2 \mathbf{I})$. In the context of autoencoders, the generator p_{θ} is often referred to as "decoder", and the inference network q_{θ} the "encoder". We then obtain the loss function as follows:

$$\mathcal{L}(\theta) = -\mathbb{E}_{\epsilon \sim q_{\theta}}[\log p_{\theta}(G_s|G_c, \epsilon)] + KL(p(\epsilon)||q_{\theta}(\epsilon|G_s, G_c)) \quad (2)$$

The first term and second term in 2 are usually referred to as the reconstruction loss ($\mathcal{L}_{\text{recon}}$) and the KL loss (\mathcal{L}_{KL}) respectively. Minimizing the loss 2 is actually maximizing a lower bound on the likelihood function 1.

The encoder $q_{\theta}(\epsilon|G_s)$, decoder $p_{\theta}(G_s|G_c, \epsilon)$, as well as the prior network $p_{\theta}(\epsilon|G_c)$ are all parameterized using graph convolutional neural networks (GNN). The architecture is shown in Figure 5.

Before entering the graph convolutional network, we perform the following transformations to the input graph $G = (V, E)$:

- Virtual bonds are added to capture remote connectivity relationship. Specifically, we add new bonds between atom pairs separated by two or three bonds, similar to our previous works.¹⁸ We also create new bond types for those virtual connections in order

to separate them from real chemical bonds. The molecular graph with virtual bonds are denoted as $G^{(1)} = (V^{(1)}, E^{(1)})$.

- $G^{(1)}$ is then transformed into a new graph $G^{(2)} = (V^{(2)}, E^{(2)})$ by treating atoms and bonds in $G^{(1)}$ equally as nodes in $G^{(2)}$. In other words, we have $V^{(2)} = V^{(1)} \cup E^{(1)}$, and $E^{(2)} = \{\{v, e\} | v \in V^{(1)}, e \in E^{(1)} \text{ and } v \in e\}$.

After those transformations, the graph G'' is then send to the graph convolutional network as input. For each convolutional layer, a similar architecture is adopted to:¹⁸

$$\mathbf{h}_v^{l+1} = \mathbf{b}^l + \Theta^l \mathbf{h}_v^l + \sum_{v' \in N_{G^{(2)}}(v)} \Phi^l \mathbf{h}_{v'}^l \quad (3)$$

Where \mathbf{h}_v^l and \mathbf{h}_v^{l+1} are features for node v at layer l and $l + 1$, $N_{G^{(2)}}(v)$ is the set of neighbors of node v in graph $G^{(2)}$. \mathbf{b}^l , Θ^l and Φ^l are weights for layer l . DenseNet is used as³¹ the overall architecture for the encoder, decoder and prior. The number of dense layers is set to be 20. At each layer, the number of bottleneck features is set to 72, and the growth rate is set to 24. We use elu as activation function.

The model is validated using holdout method. 80% of scaffolds are used for training (denoted as S^{train}), and the remaining 20% is used for testing (denoted as S^{test}). The metrics used for test set evaluation is discussed in detail in . The mini-batches $B = \{s_i, c_i\}_{i=1}^{|B|}$ used at each step for model training is constructed by first sampling the scaffolds ($\{s_i\}_{i=1}^{|B|}$) are then finding their corresponding cyclic skeleton $c_i = C(s_i)$. Naive VAE tends to suffer from the problem of posterior collapse. To encourage the model to encode more information into the latent variable, we experimented several attempts, including KL-annealing (proposed in) and³² β -VAE (proposed in³³).

AdaBound is used for model optimization, with initial learning rate set as 1×10^{-3} , and the finial learning rate as 0.1. This means that the optimizer will gradually anneal from an Adam optimizer with learning rate 1×10^{-3} to a SGD optimizer with learning rate 0.1. The gradient is clipped to $[-3, 3]$ to improve model stability. The dimension of latent variables

ϵ_v, ϵ_e are set to be 10. We performed experiments with more latent variables, but found little improvement in model performance.

Scaffold-based molecule generation

Now we introduce the model used for scaffold derivatization. The central goal of this task is to reconstruct the side-chains based on the structural information of the scaffold. Formally speaking, we are modeling the conditional distribution $p_{\theta}(x|s)$, where s is the scaffold and x is the full molecule. The generation process of side-chain follows large from our previous work⁽¹⁸⁾. The major difference is that for scaffold-based generation, the process starts from the graph of the given scaffold, instead of an empty graph (see Figure 6). The model builds the molecule in a step-by-step fashion. At each step, the model needs to decide which of the following actions to perform: (1) append a new atom to the graph, (2) connecting two existing nodes or (3) to terminate the generation process. The architecture of graph convolutional layer is similar to that used in.¹⁸ In terms of the model architecture, a 20 layer densenet is used in this model, similar to . The growth rate is set to 24, and the number of features in each bottleneck layer is set to 96. We use the likelihood-based loss function for model optimization. Importance sampling is used to improve the performance of the model (following¹⁸). The value for the hyperparameter k (the number of samples generated from importance sampling) and α (parameter controlling the degree of uncertainty in route sampling) is set as 5 and 0.5 respectively.

Note that our proposed model share similarity with that by Lim et. al. Both methods share the idea to grow the molecule directly from the scaffold. The primary difference between the models, on the other hand, lies in the dataset used. Beside including Bemis-Murko scaffolds of molecules, we also included all its sub-scaffolds within our dataset (under the definition of HierS, see for details). This treatment will have two advantages for the model. First of all, expanding the scaffold set \mathcal{S} will reduce the chance of missing potential bioactive scaffolds, making the dataset more fitted to the practical need. Secondly, the

definition of Bemis-Murko scaffold have excluded all ring-based structures from the side-chain, making it overly restricted for situations in medicinal chemistry. By including the sub-scaffolds, we can significantly increase the structural diversity of the substituents in the scaffold, thereby expanding the practicality of our model.

Model validation is performed in the following two ways:

Holdout validation

Holdout method is mainly used to obtain a overall view of the model’s performance. The set of all molecules is split into two portions: the training set (80%) and the test set (20%), used respectively for model optimization and evaluation. Note that is method will result in an overlap of scaffold set between the training and test set, therefore can not be used to examine the model’s ability of generalizing to new scaffolds.

Leave-one-out validation

Leave-one-out validation is carried out in the following way: Given a scaffold of intrest, we gather all molecules containing this scaffold as substructure, and exclude those molecules from the training set. Following this method, there will be no overlap of scaffolds and molecules between training and test set. However, it is impractical to perform such validation to all 338,932 extracted scaffolds. Therefore, we selected three scaffolds for case study, as shown in Figure 6. All scaffolds selected are privileged scaffolds for G-protein-coupled receptors (GPCRs) .

Model optimization is performed using the Adam optimizer. The learning rate is set to 0.001 in the first step, and decay at a rate of 0.99 for each 100 step, until the minimum learning rate 5×10^{-5} is reached. Regularization techniques such as dropout or weight decay is not used in this model. To stablize training, the gradient is clipped to $[-3.0, 3.0]$ at each optimization step. Training is performed for 50,000 iterations, taking roughly 20 hours to complete.

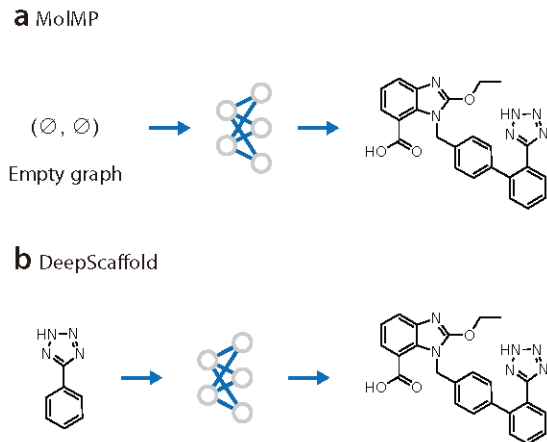


Figure 6: The generation process. **a.** Unconditional generative models (such as MolMP) starts molecule generation from empty graph $G_0 = (\cdot, \cdot)$. **b.** DeepScaffold starts molecule generation directly from scaffold.

At each step, we need to sample a mini-batch of scaffold-molecule pairs ($B = \{s_i, m_i\}_{i=1}^{|B|}$) from the training set. The batch size $|B|$ is set to 128. Note that there are many different ways to perform the sampling from the training set. For example, we can first sample a set of scaffolds $\{s_i\}_{i=1}^{|B|}$ and then assign each scaffold s_i with a molecule drawn from $M(s_i)$. We can also sample molecule first and scaffold next. The impact of different sampling algorithm is analyzed in [supporting information] The result can be summarized as follows: (1) If we place equal weight to each scaffold, the molecules will be sampled disproportionately. (2) If we place equal weight to each molecule, the scaffolds will then be sampled disproportionately. In a word, it is quite difficult to balance both scaffold and molecule. As a result, we constructure each mini-batch using a mixture of samples from both sampling methods. Here, we use a equal weight for each sampling method. In future works, the weight can be treated as a hyperparameter and be subjected to optimization and tuning.

Evaluation

Generating scaffolds from cyclic skeletons

We use the following metrics for model evaluation:

Reconstruction loss, KL loss and total loss VAE learn the generative model by trying to achieve the best reconstruction using least information. The reconstruction loss $\mathcal{L}_{\text{recon}}$ measures the accuracy of reconstruction for the autoencoder, while the KL loss \mathcal{L}_{KL} measures the amount of information stored inside the latent variable. The total loss $\mathcal{L}_{\text{total}}$, which is also used during the model training, is the sum of reconstruction loss and KL loss.

Chemical validity Given a cyclic skeleton c , we measure the chemical validity of output scaffolds generated from skeleton c . The validity of a given molecule is evaluated using the `Chem.Sanitize` API provided by RDKit. The validity is measured by the percent valid output calculated as follows:

$$P_c^{\text{valid}} = N_c^{\text{valid}} / N_c^{\text{total}} \quad (4)$$

where N_c^{valid} is the number of valid outputs and N_c^{total} is the number of total outputs. Those values are averaged among all cyclic skeletons, and the final value \bar{P}_{valid} is reported.

Evaluating scaffold-diversification model

In order to evaluate the performance of the scaffold-based molecular diversification model, we gather all scaffolds occurred inside the test set, and remove those with less than 10 corresponding molecules. After obtaining the set of scaffold to be evaluated (denoted as S_{test}), 10,000 sample molecules are generated for each scaffold, and the evaluation of those samples are carried out using the following metrics.

Chemical validity and uniqueness We first measure the chemical validity and uniqueness of the generated molecules. The validity of a given molecule is evaluated using the `Chem.Sanitize` API provided by RDKit. For a given scaffold s , we obtain the number of valid outputs (denoted as N_s^{valid}), and divide it with the total number of generated molecules (denoted as N_s^{total}). The percentage of valid outputs are calculated using 5.

To calculate the uniqueness, we remove all duplicated molecules from the valid outputs, and calculate the number of remaining molecules (denoted as N_s^{uniq}). The uniqueness is

calculated using 6.

$$P_s^{\text{valid}} = N_s^{\text{valid}} / N_s^{\text{total}} \quad (5)$$

$$P_s^{\text{uniq}} = N_s^{\text{uniq}} / N_s^{\text{valid}} \quad (6)$$

P_s^{valid} and P_s^{uniq} scores are calculated for each scaffold inside the test dataset, and the average value of the two metrics (\bar{P}_{valid} and \bar{P}_{uniq}) are reported. The distribution of the two metrics among all test set scaffolds is also reported. In addition, we will discuss how scaffold size would affect those two performance metrics.

Distribution of molecular properties Next, we investigate the model’s ability to correctly model the distribution of several important molecular properties. Here we consider the following three properties: molecular weight (denoted as MW), log partition coefficient (denoted as $\log P$) and the drug-likeness score (measured by QED²⁸). All properties above can be calculated using RDKit.

For each scaffold s in the test set, we compare the mean and standard deviation of each property (MW , $\log P$ and QED) between the molecules generated and molecules in the test set. Previous studies have used metrics such as D_{KL} and D_{JD} to quantify the difference. The approach adopted here is simpler, but offers higher interpretability compared with D_{KL} and D_{JD} . For a quantitative evaluation, we instead use maximum mean discrepancy (MMD), as discussed in .

Diversity Output diversity is another important metric for evaluating molecular generative models. Although, as discussed in , the standard deviation of molecular property could, in some extent, reflect the structural diversity of the generated outputs, a more rigorous definition of structural diversity is needed for a quantitative evaluation. Here, we adopt the formulation of internal diversity proposed by Benhenda et. al.³⁴ Supposed the molecules are sampled from a molecule distribution $x \sim p(x)$, the structural diversity of this distribution can be defined as:

$$I = 1 - \mathbb{E}_{x,y \sim p} [k(x, y)] \quad (7)$$

Where $k(x, y)$ is the similarity of the two molecules x and y . Here, we use the tanimoto score of the Morgan fingerprints between the two molecules as the similarity measurement. Intuitively speaking, the structural diversity of p is defined as one minus the average similarity between two randomly sampled molecules from p . We can estimate the value of I from samples $\{x_i\}_{i=1}^N$ drawn from p :

$$\hat{I}_U = 1 - \frac{\sum_{i=1}^N \sum_{j=1, j \neq i}^N k(x_i, x_j)}{N(N-1)} \quad (8)$$

It can be proved that \hat{I}_U is an unbiased estimator of I . Note that this estimator is slightly different from that originally proposed by Benhenda et. al.:³⁴

$$\hat{I}_V = 1 - \frac{\sum_{i,j=1}^N k(x_i, x_j)}{N^2} \quad (9)$$

It can be shown that \hat{I}_V is in fact equals to $\frac{N-1}{N} \hat{I}_U$, and therefor a biased V-statistics for I . Also, it can be shown that the bias of \hat{I}_V depends on the sample size N , and will be larger in smaller datasets. This could be problematic for two ways: First, many scaffold in the test set have only a small number of corresponding molecules, which may increase the bias. Second, the sample size (N) of the test set is usually smaller than that of the generated samples, which will bring additional bias to the result. Therefore, the U-statistics \hat{I}_U is instead used in this paper for the calculation of internal diversity.

Maximum mean discrepancy (MMD) The central task of scaffold-based diversification is to model the conditional distribution $p(x|s)$ of molecular structure x given the scaffold s . Therefore, the most natural way of evaluating such model would be measuring the dissimilarity between the ground truth distribution $p_d(x|s)$ and the modeled distribution $p_g(x|s)$. Maximum mean discrepancy (MMD) is one of such metrics that have been widely applied in generative modeling (both for model training³⁵ and evaluation³⁶). Different from other

metrics, such as Jensen–Shannon divergence (JSD), Wasserstein distance (WD)³⁷ or Frechet ChemNet distance (FCD),³⁸ MMD does not require additional discriminator or predictor in order to be evaluated, which makes it much easier to calculate.

Given the samples from two probability distribution $\{x_i\}_{i=1}^N \sim p_d$, $\{y_i\}_{i=1}^M \sim p_g$, the MMD between the two distribution can be estimated as:

$$\hat{D} = \frac{1}{N(N-1)} \sum_{i=1}^N \sum_{j=1, j \neq i}^N k(x_i, x_j) + \frac{1}{M(M-1)} \sum_{i=1}^M \sum_{j=1, j \neq i}^M k(y_i, y_j) - \frac{2}{MN} \sum_{i=1}^N \sum_{j=1}^M k(x_i, y_j) \quad (10)$$

Where $k(\cdot, \cdot)$ is the kernel function. Similar to , we choose the tanimoto similarity between molecules as k . It can be proved that tanimoto similarity is in fact a legitimate kernel function.³⁹

One of the most important application the model is the design of molecule based on privileged scaffolds. Ideally, given a known bioactive scaffold, the generated molecule should also be bioactive. To test whether the model possess such desirable property, we examine:

- The ability for the generative model to reproduce kown active moleculces
- The (predicted) bioactivity of the output molecules for the target.

The rate of reproduced active compounds First of all, the rate reproduced active molecules (denoted as R) for GPCRs is reported. Specifically, we collect all molecules that are active against at least one target in the GPCR family (denoted as the set T_{GPCR}), and examine how many of them appears in the set of molecules sampled from the model(denoted as M_s):

$$R_{\text{GPCR}} = \frac{|M_s \cap T_{\text{GPCR}}|}{|T_{\text{GPCR}}|} \quad (11)$$

We also investigate the ability for the model to reproduce known drugs, by collecting all drugs (denoted as T_{drug}) from the test set, and calculate the ratio R_{drug} :

$$R_{\text{drug}} = \frac{|M_s \cap T_{\text{drug}}|}{|T_{\text{drug}}|} \quad (12)$$

Docking Next, we report the predicted activity of output molecule for GPCRs. It is impractical to evaluate the output molecule against all targets in the GPCR family. Instead, we choose Dopamine Receptor D2 (DRD2) as a representative, which is a well studied target for antipsychotic drugs.⁴⁰ The predicted activity for DRD2 is calculated using docking. The bioactivity model for DRD2 is built following [supporting information]:

For each bioactive scaffold selected for GPCRs, a comparison of docking scores was carried out between four sets of compounds: (1) samples generated by the model, (2) molecules inside the test set, (3) known actives for DRD2 and (4) randomly sampled molecules from ChEMBL. A well performing generative model should result in a similar distribution of docking scores between (1) and (2). Also, the average score for (1) should be close to (3), and better than (4).

Structural distribution of side-chains Given the set of generated molecules given a scaffold, users can further filter the result by adding requirement on the properties of side-chains attached to the scaffold. Since different users may require different type of substitution in different locations, the model needs to generate a diverse set of side-chain configurations in order to handle the user’s requirements efficiently. Therefore, for each scaffold in the leave-one-out evaluation (see), we analyse the location and size of each side-chain in the generated molecules in order to evaluate the diversity of side-chains. We also compare the result with test set molecules to determine the quality of the generated samples.

Results

Generated samples

Before diving into model’s performance, we present a brief view of DeepScaffold by showcasing several generated molecules from cyclic skeletons as well as classical scaffolds using the model. The result is demonstrated in Figure 7. Two cyclic skeleton, scaffold 4 (Figure 7 g), with a relatively simple sturcture, as well as the more complexed scaffold 1 (Figure 7 b), are selected from the hold out test set. For each scaffold, we generate two classical scaffolds (scaffold 2 (Figure 7 c) and scaffold 3 (Figure 7 e) for scaffold 1, as well as scaffold 5 (Figure 7 h) and scaffold 6 (Figure 7 j) for scaffold 4 and structural derivivication is performed on those structure (Figure 7 d,f,i,k).

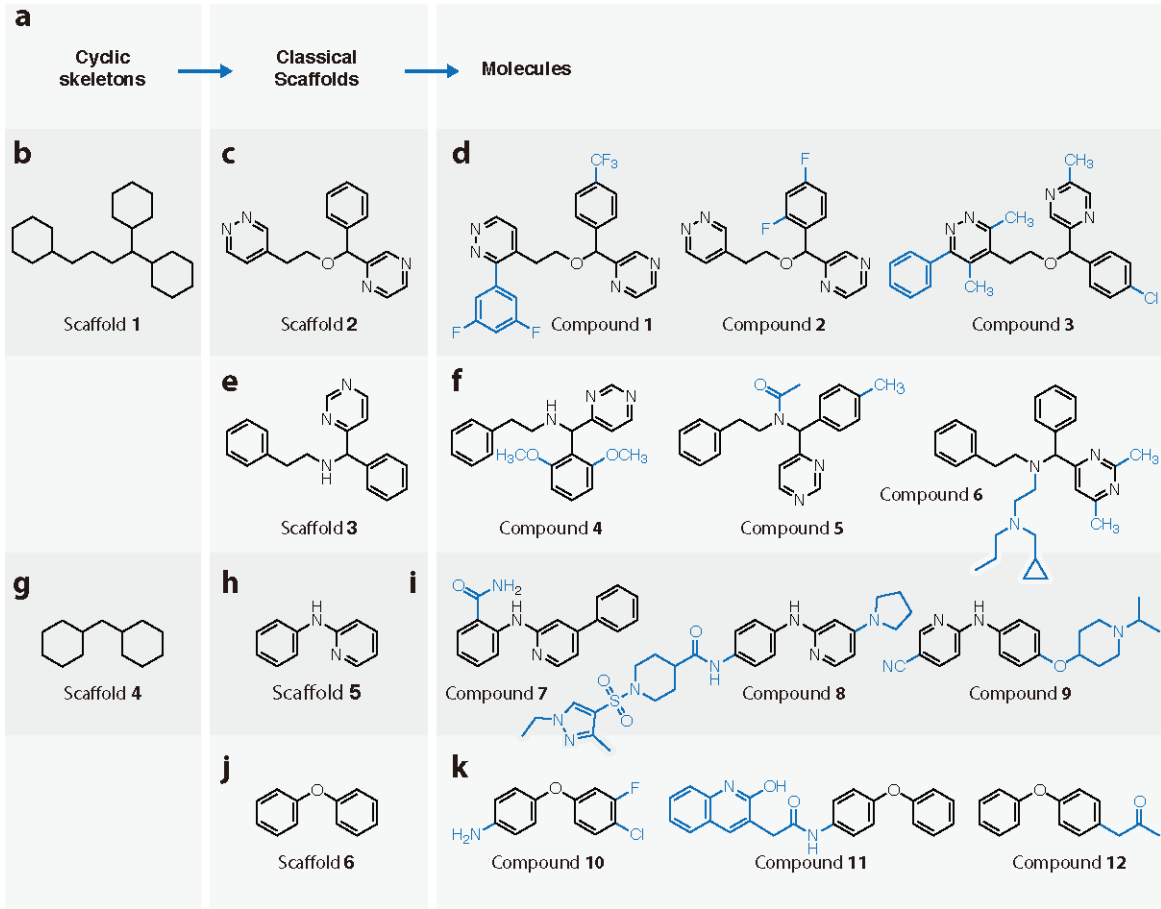


Figure 7: Generated samples from DeepScaffold.

Generating scaffolds from cyclic skeletons

The performance of the proposed model is evaluated following , with results shown in 1.

Table 1: Generating scaffolds from cyclic skeletons

Model	%valid	%recon	\mathcal{L}_{KL}	$\mathcal{L}_{\text{recon}}$	$\mathcal{L}_{\text{total}}$
β -VAE ($\beta = 0.5$)	82.50%	61.00%	9.82	1.11	10.93
β -VAE ($\beta = 0.1$)	80.70%	91.30%	14.15	0.23	14.38
VAE + KL annealing	76.80%	10.00%	5.02	4.38	9.4
VAE	68.50%	6.32%	3.37	6.06	9.43

First of all, it is shown that approaches such as KL-annealing and β -VAE all showed positive results in solving posterior collapse. Both VAE + annealing and β -VAE are capable of achieving higher \mathcal{L}_{KL} . Notably, by using annealing, the model can achieve a slightly better $\mathcal{L}_{\text{total}}$ with a much higher \mathcal{L}_{KL} . In terms of the output validity, β -VAE (with β value set to 0.5) is able to achieve the best performance of 82.5%. Interestingly, the output validity is not always consistent with the performance measured using $\mathcal{L}_{\text{total}}$. In the future, we plan to utilize more recent techniques in VAE training in order to improve the result, such as using more complexed prior⁴¹ posterior.⁴²

Scaffold derivation

Validity and uniqueness

The performance of scaffold-based molecular diversification in terms of validity and uniqueness is summarized in Figure 8. Among all scaffolds, the average percentage of valid output (\bar{P}_{valid}) is 98.9%, and the average percentage of unique output is 69.1% (\bar{P}_{uniq}), as shown in Figure 8. It is immediately noticed that the result in \bar{P}_{valid} and \bar{P}_{uniq} is significantly different from the results produced by the unconditional version of the model with similar

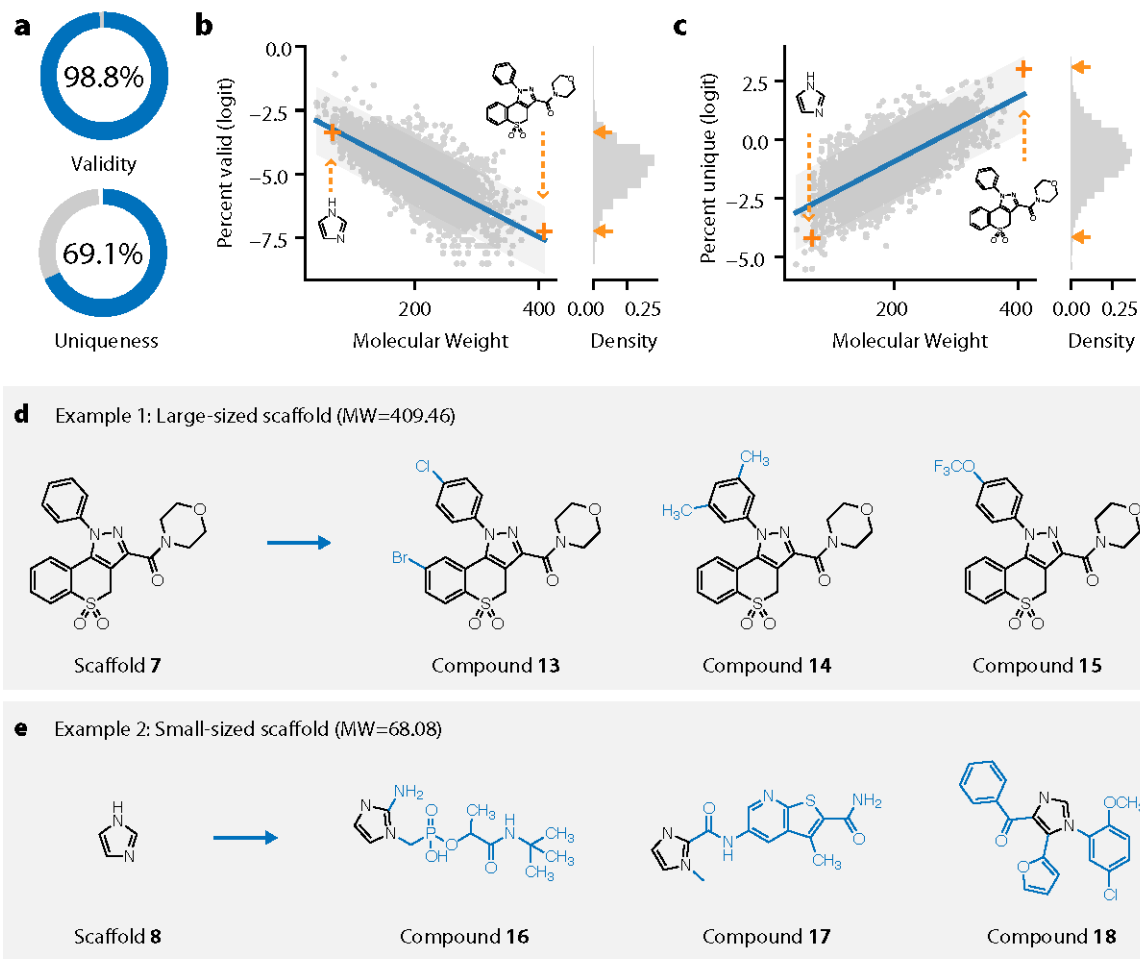


Figure 8: Sample validity and uniqueness. **a**. The average validity (98.8%) and uniqueness (69.1%) among all scaffolds. **b**. The relationship between molecular weight of each scaffold and the (logit) percent valid output. **c**. The relationship between molecular weight for each scaffold and (logit) percent unique output. **d-e**. Several generated samples using scaffolds with **d**. high molecular weight and **e**. low molecular weight.

architecture.¹⁸ Specifically, scaffold-based model can achieve a higher percent valid value, while having a lower percent unique value. A similar result was reported by Lim et. al.²⁶ using a different dataset including BM scaffolds.

To better understand the phenomenon, we further investigate the relationship between the scaffold size (measured by the molecular weight of the scaffold MW_s) and the performance of the two metrics. The result is shown in Figure 8 and Figure 8. It can be shown that MW_s is positively correlated with P_s^{valid} (correlation coefficient $r = 0.73$, significance level $p < 0.001$

), while negatively correlates with P_s^{uniq} (correlation coefficient $r = -0.66$, significance level $p < 0.001$). This means that larger scaffolds tends to have higher output validity, but lower uniqueness. The result is infact inline with the mode of thinking in medicinal chemistry: for smaller scaffold, there are usally a plenty of room for sturctural diversification, while for larger scaffolds, in order to achieve higher drug-likeness and synthetic accessibility, the size and diversity of structural modification is much more restricted, resulting a higher chance of duplicates. Also, smaller side-chains means fewer generation steps, which will therefore reduce the chance of validity violation during generation. Two representitive scaffolds are chosen from the test scaffold set and are shown in Figure 8 and Figure 8. Consistant with the analysis above, the side-chains attached to the smaller scaffold is larger and more diverse, and those attached to the larger scaffold have much simpler structure.

The discussion above also provides some important insight into how future benchmarks should be constrctured for this type of model. First of all, since the evaluation metrics such as P_s^{valid} and P_s^{uniq} depends on the scaffold s chosen for evaluation, it is important to use a common scaffold set as test set during model comparison. Secondly, it will be better to perform the evaluation in a per-scaffold fasion. Specifically speaking, instead of comparing the average validity and uniqueness between models, it will be better to perform paired test of those metrics.

Molecular properties

Next, the distributions of molecular properties for generated molecules are analyzed and compared with that in the test set. The results are summarized in Figure 9. Each point in the scatter point corresponds to a scaffold in the test set. It’s horizontal coordinate indicates the statistics (mean or standard deviation) of a molecular property (MW, LogP or QED) of generated molecules, while its y coordinate indicates that statistics for the test set molecules. Scaffolds having more than 400 corresponding molecules in the test set are lighted in blue.

We first examine the mean statistics of molecular properties. Form Figure 9, it can be

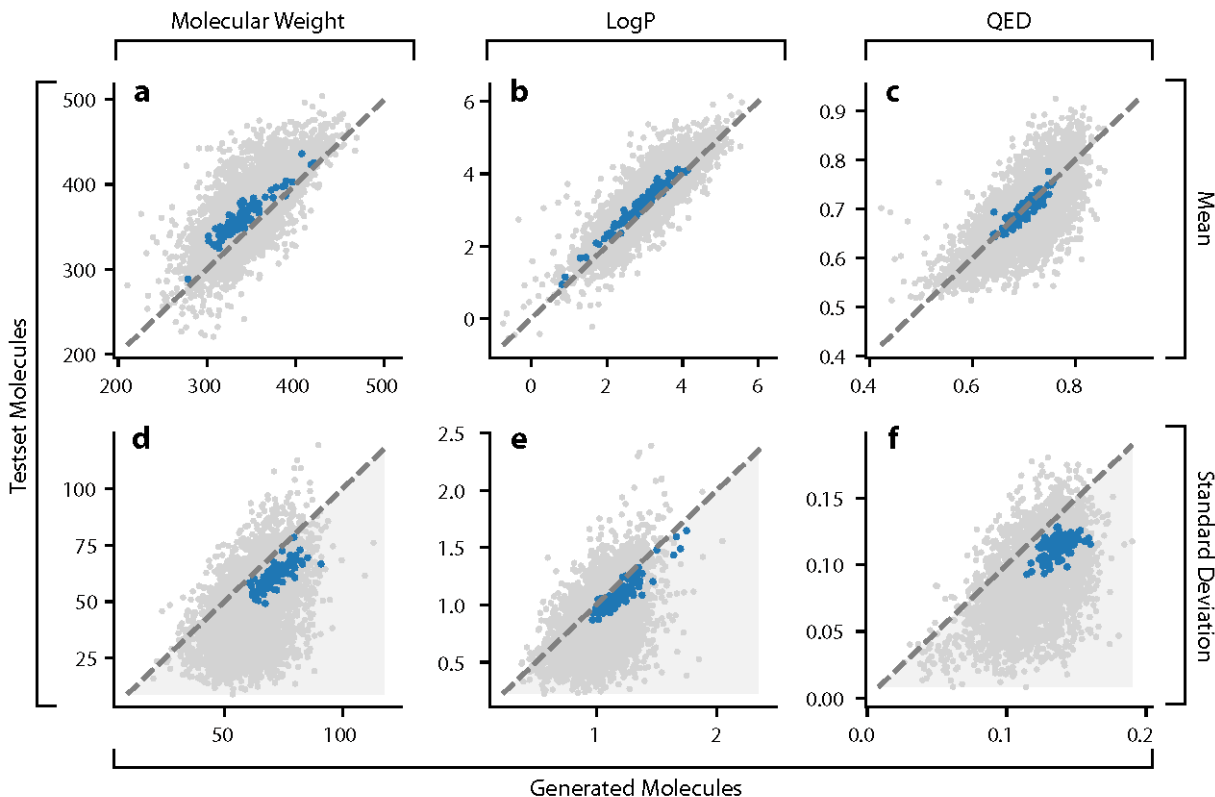


Figure 9: Comparing the distribution of several molecular properties (MW, LogP and QED) between generated and test set molecules. For each subplot, the horizontal coordinate indicates the statistics (**a-c** for mean and **d-f** for standard deviation) of a molecular property (**a** and **d** for MW, **b** and **e** for LogP, **c** and **f** for QED) of generated molecules, while its y coordinate indicates that statistics for the test set molecules. Scaffolds with more than 400 corresponding molecules (that is, $|\mathcal{M}(s)| > 400$) are highlighted in blue.

observed that, for all three properties, the points in the scatter plot lies relatively close to the diagonal line, demonstrating that the model is performing well in modeling the means of those properties. It is also noted that scaffolds with more molecules (highlighted in blue) lies much closer to the diagonal line compared with other scaffolds. This may indicate a better performance in scaffolds with more data points.

However, in terms of standard deviation, there is a large discrepancy between the generated and test samples. It is observed that a large number of data points lies below the diagonal line, which indicates that the generated molecule usually have a more dispersed distribution of molecular properties. This is in fact a result of higher structural diversity of

output molecules, as is shown in . Again, highlighted point is observed to lie much closer to the diagonal line, showing that the model performs much better on those scaffolds compared with the rest.

Molecule diversity

We subsequently analyze the internal diversity of the sampled and test set molecules, with results summarized in Figure 10. Similar to the result showed in Figure 10, we have observed that most data points lie below the diagonal line, indicating a higher structural diversity of sampled molecules compared with test set molecules. Also, a similar result is observed that scaffolds with more data in the training set performs much better compared with other scaffolds (see the data points highlighted in blue).

MMD

The result for MMD is shown in Figure 10. The grey curve shows the distribution of MMD among all test set scaffolds, while the blue curve shows the distribution of MMD among scaffolds with more than 400 related molecules. It can be immediately observed from the figure that the model performs significantly better for scaffolds included in the blue line.

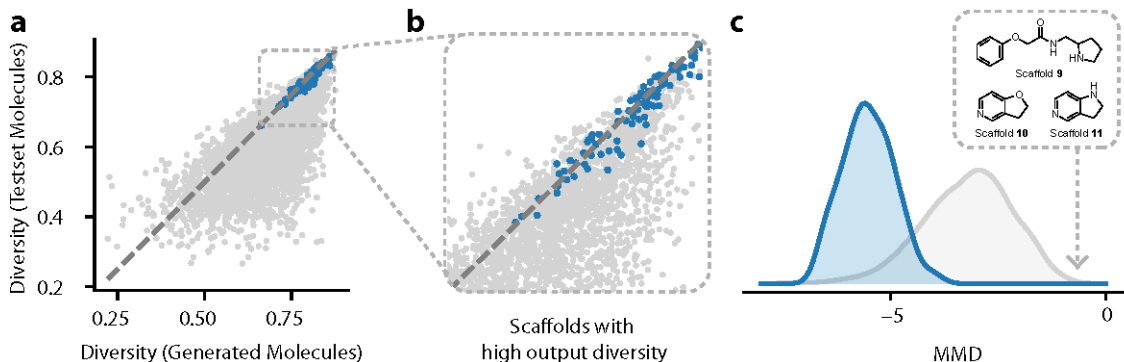


Figure 10: Internal diversity and MMD. **a.** Comparing the internal diversity between generated molecules and testset molecules. Scaffolds with more than 400 corresponding molecules (that is, $|\mathcal{M}(s)| > 400$) are highlighted in blue. **b.** Scaffolds with high output diversity. **c.** The distribution of MMD among all scaffolds in the test set. Scaffolds with more than 400 corresponding molecules are highlighted in blue.

Analysing bad-cases

In summary, the evaluation results reported in the above sections have lead to the following conclusions regarding to the model’s performance:

- With a given scaffold, molecules generated by the model tend to be more structually diversified compared with the molecules containing that scaffold in the test set
- The distribution of generated molecules matches better with that of the test set molecules for scaffolds that occurs more frequently.

In order to get a better understand those phenomenons, we performed a bad-case analysis considering scaffolds with lowest MMD values, as demonstrated in Figure 11. Generated molecules for those scaffolds are shown in Figure 11, while molecules containing those scaffolds in the test set are shown in Figure 11.

As we examine the results in Figure 11, we can immediately notice the low structural diversity for the test set molecules. Intrestingly, after inspecting the origin of those molecules in the ChEMBL dataset, we found that those molecules are mostly collected from a single publication or a single assay: All molecules containing scaffold **9** is originated from the assay ChEMBL3707834, and all molecules containing scaffold **10** is originated from the assay ChEMBL3705917. 89% of molecules containing scaffold **11** is collected from the publication ChEMBL1144160. In other words, for each scaffold shown in Figure 11, its corresponding molecules are largely design by a same group of researchers under a same target.

The observations above can offer an explanation to the seemly bad performance of model. It can be concluded that the test set for scaffold **9-11** suffers from the non-random-sampling bias: the molecules is sampled from a much more restricted chemical space that reflects the perference of a specific research or publication. Therefore, the performance of the model will be underestimated, resulting in high MMD values, as well as large discrepancy between structural and property distributions. On the contrary, a higher diversity in generated

molecule is actually a sign that the model did not memorize the side-chain distribution for each scaffold, indicating a high generalizability.

The foregoing discussion proposes a challenge for model evaluation in scaffold-diversification tasks. In order to obtain a good assessment for the model’s performance, it is necessary to use a test set that is unbiased in molecule distribution. Future research may explore the potential of developing an unbiased benchmark set for scaffold-diversification models. Another solution would be introducing sample weight during evaluation to mitigate the non-random-sampling bias, which will be leaved for future researches.

Case study: privileged scaffolds for GPCRs

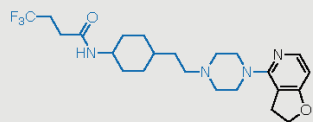
As discribed in , three privileged scaffolds for GPCRs (shown in Figure 12) are selected for case study. We performed leave-one-out evaluation for each scaffold, with the results summarized in 2 and Figure 12.

The model performs well on the precentage of valid outputs, with values closing to 100%. The uniqueness for scaffold **12** and **13** is 86.6% and 87.7% respectively, while for **14**, the value is of 45.4%. This smaller value might be resulted from the higher structural complexity of scaffold **14**, which may ristic the chemical space of the side chains. Similar to the results demonstrated in and generated molecules have a wider distribution of MW, LogP and QED, and is more structurally diversified compared to real samples. In terms of MMD, we found that scaffold **14** have a significantly lower MMD value compared with scaffold **12** and **13**. The high MMD value can largely be contributed to the non-random-sampling bias in the test set. In fact, most scaffold containing scaffold **14** is collected from two publications (ChEMBL id: ChEMBL1008329, ChEMBL1001157), with both publication focusing on a same target called Neuropeptide Y receptor type 5 (NPY Y5).

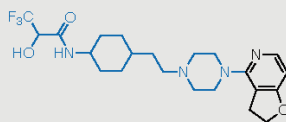
Next, we investigate the ability for the model to reproduce know active molecules against GPCRs (see results in 2). Within 10,000 samples, the model can reproduce 5.17% active molecules and 12.8% kown drugs containing scaffold **12**, 8.44% active molecules and 25%

a Case 1

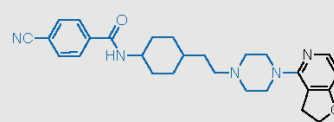
Molecule inside the test set:



CHEMBL3642772

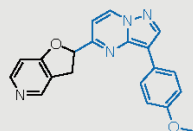


CHEMBL3642788

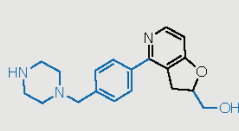


CHEMBL3642793

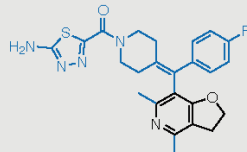
Molecules generated



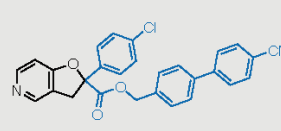
Compound 19



Compound 20



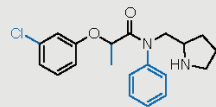
Compound 21



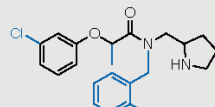
Compound 22

b Case 2

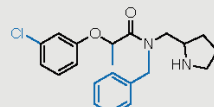
Molecule inside the test set:



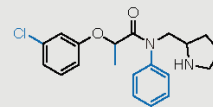
CHEMBL528332



CHEMBL482420

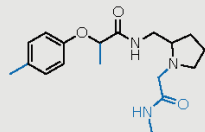


CHEMBL485090

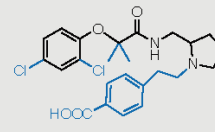


CHEMBL489403

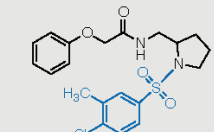
Molecules generated



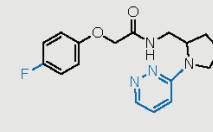
Compound 23



Compound 24



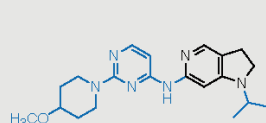
Compound 25



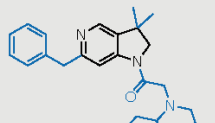
Compound 26

c Case 3

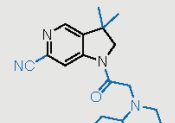
Molecule inside the test set:



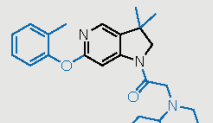
CHEMBL3354194



CHEMBL3639988

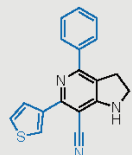


CHEMBL3699984

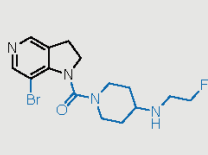


CHEMBL3699965

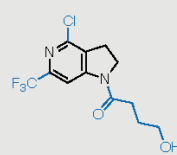
Molecules generated



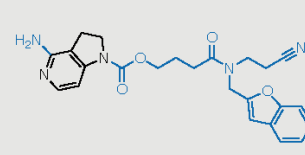
Compound 27



Compound 28



Compound 29



Compound 30

Figure 11: Demonstration of several bad-cases drawn from the test set scaffolds.

kown drugs containing scaffold **13**, as well as 15.9% active molecules containing scaffold **14**. Several reproduced drugs are shown in Figure 12. Since the model have no access to those molecules during the training phase, the results above demonstrated good potential for drug discovery based on privileged scaffolds.

Table 2: Case study: privileged scaffolds for GPCRs

	Scaffold 12	Scaffold 13	Scaffold 14
Diversity	0.166	0.187	0.485
Molecular Weight	363.6 (58.1)	384.9 (64.6)	385.3 (38.0)
LogP	4.04 (1.06)	4.01 (1.02)	3.72 (0.698)
QED	0.675 (0.114)	0.708 (0.121)	0.660 (0.0492)
MMD	0.0185	0.00875	0.154
R(actives)	0.0517	0.0844	0.159
R(drugs)	0.128	0.25	-
P_s^{valid}	0.986	0.974	0.989
P_s^{uniq}	0.866	0.877	0.454

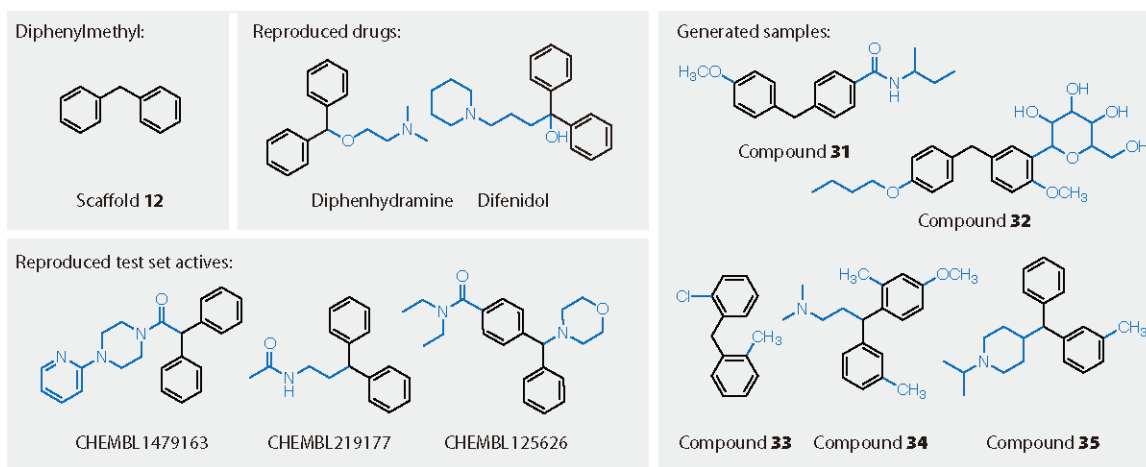
Analysing the structural distribution of side chains

Finally, we investigate the structural distribution of side chains generated by the model. We summarize the result in 13.

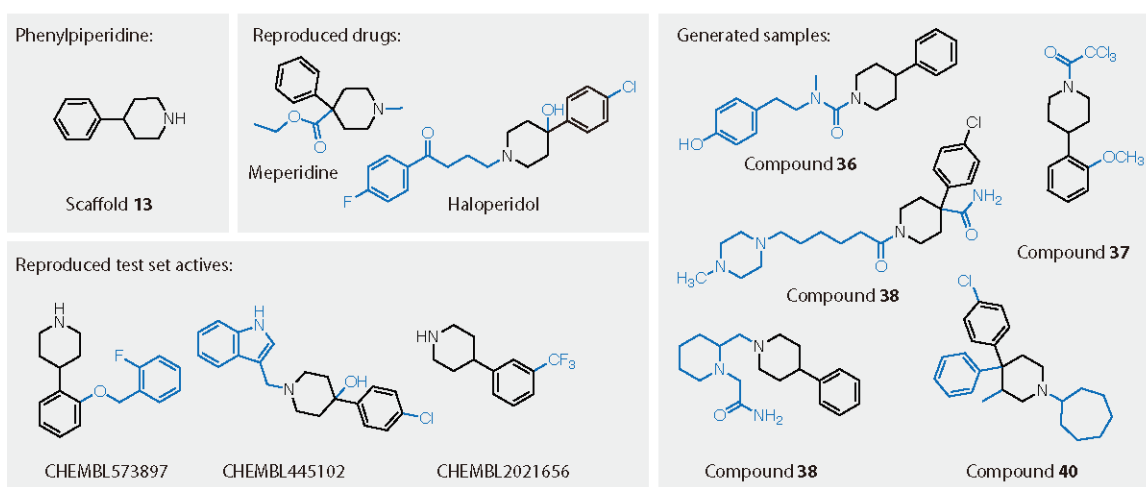
The result demonstrated a diversified substitution pattern generated from the model. Note that for scaffold **14**, the substitution only happens in location **3** for molecules inside ChEMBL (the reason for the low diversity is discussed in). But in the generated molecules, the substitution pattern is much more diverse, demonstrating high generalizability for the model.

Interestingly, it is found that the model add side-chain to nitrogen atoms more often than other locations. It is also found the size of side-chain attached to nitrogen atoms tends to be

a Scaffold 1



b Scaffold 2



c Scaffold 3

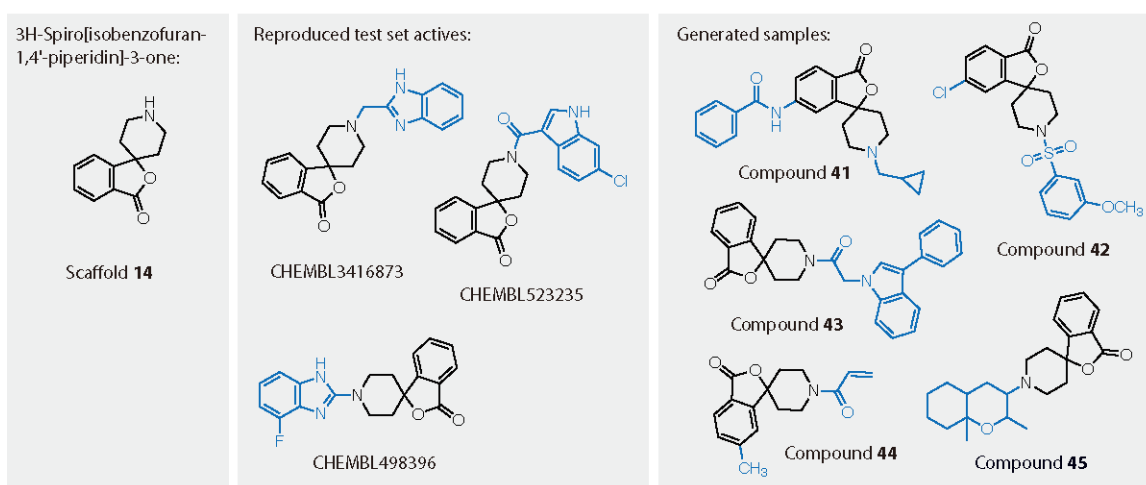


Figure 12: Generated samples and reproduced active molecules. This figure shows the generated molecules by the model given each scaffold (**a.** for scaffold **12**, **b.** for scaffold **13**, **c.** for scaffold **14**) as well as the reproduced drugs and active molecules.

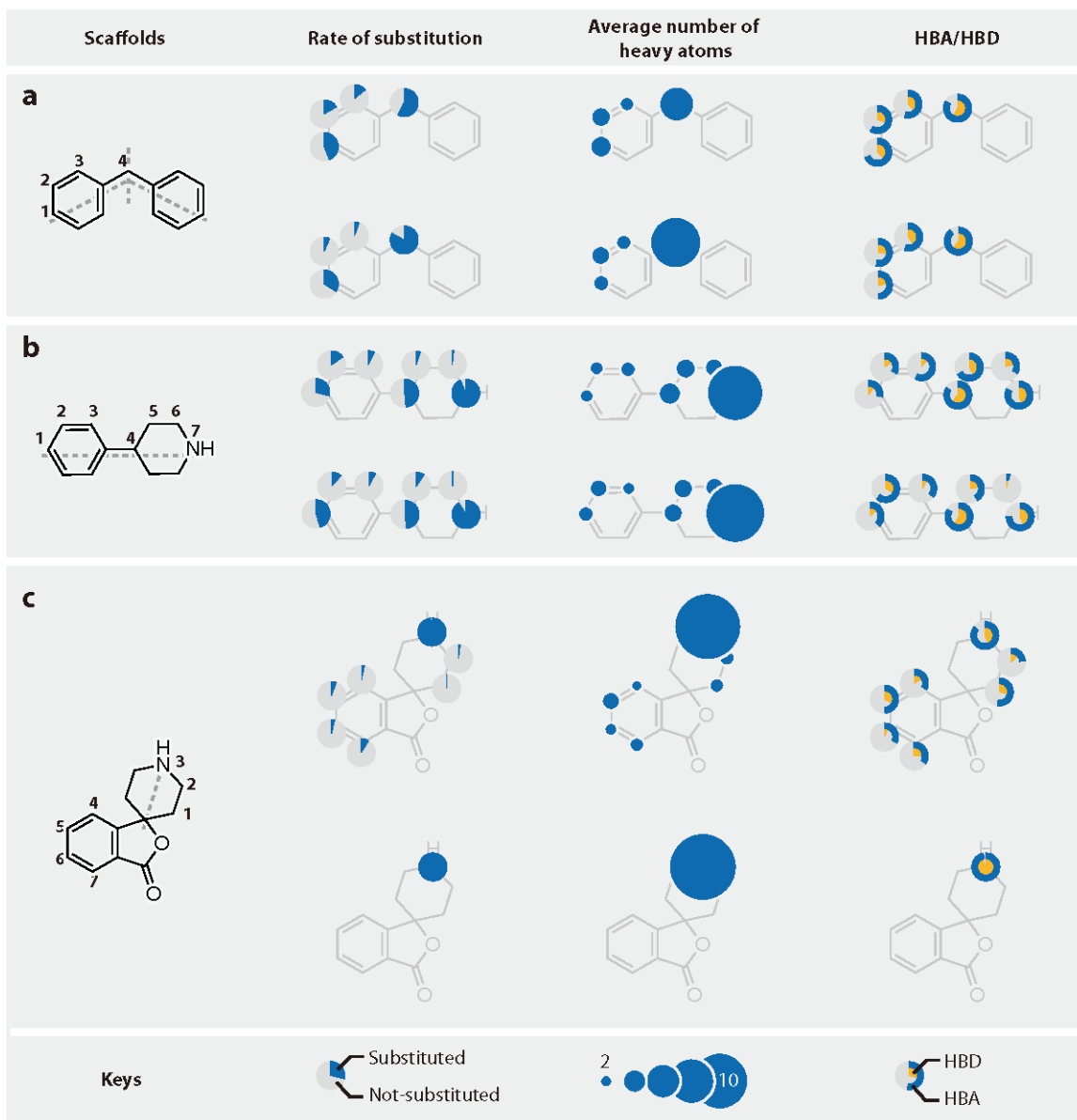


Figure 13: The distribution of side chain properties at each location for scaffold **12-14**.

much larger compared with that in other positions. Those observations could be resulted from a mixed effect of synthetic accessibility and drug-likeness.

Distribution of docking scores

The distribution of docking scores of generated molecules with DRD2 is shown in Figure 14. As demonstrated, the predicted activities of generated samples (orange) are similar to that of the test set molecules (light grey). For scaffold **13** and scaffold **14**, the pre-

dicted activity against DRD2 for generated samples are significantly higher compared with randomly sampled molecules from ChEMBL, showing that the model is good at utilizing privileged structures for generating bioactive molecules. On the other hand, for scaffold **12**, the predicted activities of generated samples could not outperform that of random ChEMBL samples. This may due to the fact that the bioactivity privilege of scaffold **12** is not as significant compared with **13** and **14**, according to the docking result. In fact, scaffold **12** is highly prevalent among molecules in ChEMBL, and could occur in compounds with different targets. This may explain the results for scaffold **12** shown above.

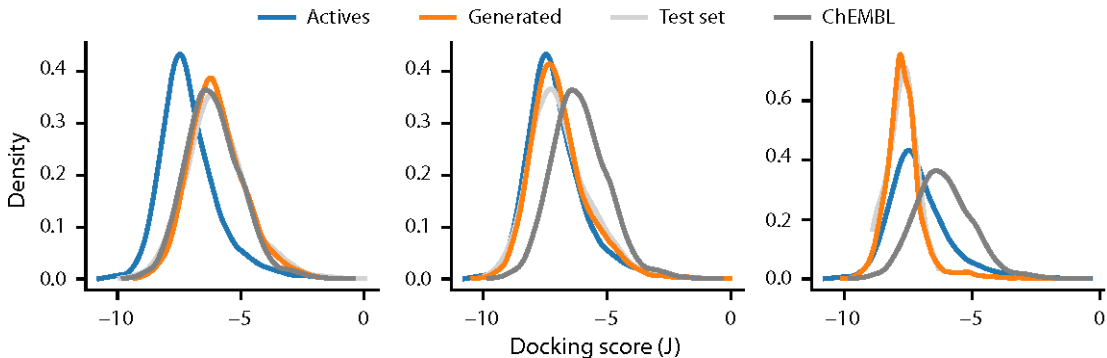


Figure 14: The distribution of docking scores. This plot shows the distribution of docking scores of three sets of molecules (active molecules, generated molecules, test set molecules and random compounds from ChEMBL) for each scaffold (**a.** scaffold **12**, **b.** scaffold **13** and **c.** scaffold **14**).

Conclusion

We proposed a comprehensive solution for scaffold-based drug discovery using deep learning. The model is capable of performing molecular design tasks based on a wide spectrum of scaffold definitions, including BM-scaffolds, cyclic skeletons, as well as scaffolds with specifications on side-chain properties. Evaluation is performed to assess the performance of the models. In addition, we chose several privileged scaffolds for GPCRs for case study, demonstrating the practical value of the model in medicinal chemical problems. We packed

the models into a command line tool, which would be available at [repo], together with the project source code.

References

- (1) Hu, Y.; Stumpfe, D.; Bajorath, J. Computational Exploration of Molecular Scaffolds in Medicinal Chemistry. *J Med Chem* **2016**, *59*, 4062–76.
- (2) Bemis, G. W.; Murcko, M. A. The properties of known drugs. 1. Molecular frameworks. *J Med Chem* **1996**, *39*, 2887–93.
- (3) Barreiro, E. J. *Privileged Scaffolds in Medicinal Chemistry*; Royal Society of Chemistry: London, 2015.
- (4) Varin, T.; Schuffenhauer, A.; Ertl, P.; Renner, S. Mining for bioactive scaffolds with scaffold networks: improved compound set enrichment from primary screening data. *J Chem Inf Model* **2011**, *51*, 1528–38.
- (5) Nakagawa, T.; Miyao, T.; Funatsu, K. Identification of Bioactive Scaffolds Based on QSAR Models. *Mol Inform* **2018**, *37*.
- (6) Varin, T.; Gubler, H.; Parker, C. N.; Zhang, J.-H.; Raman, P.; Ertl, P.; Schuffenhauer, A. Compound set enrichment: a novel approach to analysis of primary HTS data. *Journal of chemical information and modeling* **2010**, *50*, 2067–2078.
- (7) Wilkens, S. J.; Janes, J.; Su, A. I. HierS: hierarchical scaffold clustering using topological chemical graphs. *Journal of medicinal chemistry* **2005**, *48*, 3182–3193.
- (8) Koch, M. A.; Schuffenhauer, A.; Scheck, M.; Wetzol, S.; Casaulta, M.; Odermatt, A.; Ertl, P.; Waldmann, H. Charting biologically relevant chemical space: a structural classification of natural products (SCONP). *Proc Natl Acad Sci* **2005**, *102*, 17272–7.

- (9) Schuffenhauer, A.; Ertl, P.; Roggo, S.; Wetzol, S.; Koch, M. A.; Waldmann, H. The scaffold tree–visualization of the scaffold universe by hierarchical scaffold classification. *J Chem Inf Model* **2007**, *47*, 47–58.
- (10) Schafer, T.; Kriege, N.; Humbeck, L.; Klein, K.; Koch, O.; Mutzel, P. Scaffold Hunter: a comprehensive visual analytics framework for drug discovery. *J Cheminform* **2017**, *9*, 28.
- (11) LeCun, Y.; Bengio, Y.; Hinton, G. Deep learning. *Nature* **2015**, *521*, 436–44.
- (12) Hu, Z.; Yang, Z.; Salakhutdinov, R.; Xing, E. P. On Unifying Deep Generative Models. International Conference for Learning Representations.
- (13) Schneider, G.; Fechner, U. Computer-based de novo design of drug-like molecules. *Nat Rev Drug Discov* **2005**, *4*, 649–63.
- (14) Segler, M. H. S.; Kogej, T.; Tyrchan, C.; Waller, M. P. Generating Focused Molecule Libraries for Drug Discovery with Recurrent Neural Networks. *ACS Cent Sci* **2018**, *4*, 120–131.
- (15) Gomez-Bombarelli, R.; Wei, J. N.; Duvenaud, D.; Hernandez-Lobato, J. M.; Sanchez-Lengeling, B.; Sheberla, D.; Aguilera-Iparraguirre, J.; Hirzel, T. D.; Adams, R. P.; Aspuru-Guzik, A. Automatic Chemical Design Using a Data-Driven Continuous Representation of Molecules. *ACS Cent Sci* **2018**, *4*, 268–276.
- (16) Olivecrona, M.; Blaschke, T.; Engkvist, O.; Chen, H. Molecular de-novo design through deep reinforcement learning. *Journal of Cheminformatics* **2017**, *9*, 48.
- (17) Weininger, D. SMILES, a chemical language and information system. 1. Introduction to methodology and encoding rules. *Journal of Chemical Information and Modeling* **1988**, *28*, 31–36.

- (18) Li, Y.; Zhang, L.; Liu, Z. Multi-objective de novo drug design with conditional graph generative model. *J Cheminform* **2018**, *10*, 33.
- (19) Simonovsky, M.; Komodakis, N. GraphVAE: Towards Generation of Small Graphs Using Variational Autoencoders. *arXiv:1610.02920* **2017**,
- (20) Li, Y.; Vinyals, O.; Dyer, C.; Pascanu, R.; Battaglia, P. Learning Deep Generative Models of Graphs. *arXiv:1803.03324* **2017**,
- (21) You, J.; Ying, R.; Ren, X.; Hamilton, W. L.; Leskovec, J. GraphRNN: Generating Realistic Graphs with Deep Auto-regressive Models. International Conference on Machine Learning.
- (22) Jin, W.; Barzilay, R.; Jaakkola, T. Junction Tree Variational Autoencoder for Molecular Graph Generation. International Conference on Machine Learning.
- (23) De Cao, N.; Kipf, T. MolGAN: An implicit generative model for small molecular graphs. *arXiv:1805.11973* **2018**,
- (24) Aumentado-Armstrong, T. Latent Molecular Optimization for Targeted Therapeutic Design. *arXiv:1809.02032* **2018**,
- (25) Zheng, S.; Yan, X.; Gu, Q.; Yang, Y.; Du, Y.; Lu, Y.; Xu, J. QBMG: quasi-biogenic molecule generator with deep recurrent neural network. *J Cheminform* **2019**, *11*, 5.
- (26) Lim, J.; Hwang, S.-Y.; Kim, S.; Moon, S.; Kim, W. Y. Scaffold-based molecular design using graph generative model. *arXiv:1905.13639* **2019**,
- (27) Gaulton, A.; Bellis, L. J.; Bento, A. P.; Chambers, J.; Davies, M.; Hersey, A.; Light, Y.; McGlinchey, S.; Michalovich, D.; Al-Lazikani, B.; Overington, J. P. ChEMBL: a large-scale bioactivity database for drug discovery. *Nucleic Acids Res* **2012**, *40*, D1100–7.
- (28) Bickerton, G. R.; Paolini, G. V.; Besnard, J.; Muresan, S.; Hopkins, A. L. Quantifying the chemical beauty of drugs. *Nat Chem* **2012**, *4*, 90–8.

- (29) Ertl, P.; Schuffenhauer, A. Estimation of synthetic accessibility score of drug-like molecules based on molecular complexity and fragment contributions. *J Cheminform* **2009**, *1*, 8.
- (30) Kingma, D. P.; Welling, M. Auto-encoding variational bayes. International Conference for Learning Representations.
- (31) Huang, G.; Liu, Z.; Van Der Maaten, L.; Weinberger, K. Q. Densely connected convolutional networks. Proceedings of the IEEE conference on computer vision and pattern recognition. pp 4700–4708.
- (32) Bowman, S. R.; Vilnis, L.; Vinyals, O.; Dai, A. M.; Jozefowicz, R.; Bengio, S. Generating sentences from a continuous space. SIGNLL Conference on Computational Natural Language Learning.
- (33) Higgins, I.; Matthey, L.; Pal, A.; Burgess, C.; Glorot, X.; Botvinick, M.; Mohamed, S.; Lerchner, A. beta-VAE: Learning Basic Visual Concepts with a Constrained Variational Framework. *ICLR* **2017**, *2*, 6.
- (34) Benhenda, M. ChemGAN challenge for drug discovery: can AI reproduce natural chemical diversity? *arXiv:1708.08227* **2017**,
- (35) Li, C.-L.; Chang, W.-C.; Cheng, Y.; Yang, Y.; PÅszczos, B. Mmd gan: Towards deeper understanding of moment matching network. Advances in Neural Information Processing Systems. pp 2203–2213.
- (36) Jiwoong Im, D.; Ma, A. H.; Taylor, G. W.; Branson, K. Quantitatively Evaluating GANs With Divergences Proposed for Training. International Conference on Learning Representations.
- (37) Arjovsky, M.; Chintala, S.; Bottou, L. Wasserstein GAN. International Conference on Learning Representations.

- (38) Preuer, K.; Renz, P.; Unterthiner, T.; Hochreiter, S.; Klambauer, G. Frechet ChemNet Distance: A Metric for Generative Models for Molecules in Drug Discovery. *J Chem Inf Model* **2018**, *58*, 1736–1741.
- (39) Gower, J. C. A general coefficient of similarity and some of its properties. *Biometrics* **1971**, 857–871.
- (40) Madras, B. K. History of the discovery of the antipsychotic dopamine D2 receptor: a basis for the dopamine hypothesis of schizophrenia. *Journal of the History of the Neurosciences* **2013**, *22*, 62–78.
- (41) Chen, X.; Kingma, D. P.; Salimans, T.; Duan, Y.; Dhariwal, P.; Schulman, J.; Sutskever, I.; Abbeel, P. Variational lossy autoencoder. International Conference on Learning Representations.
- (42) Kingma, D. P.; Salimans, T.; Jozefowicz, R.; Chen, X.; Sutskever, I.; Welling, M. Improved variational inference with inverse autoregressive flow. Advances in Neural Information Processing Systems. pp 4743–4751.